Improvements in cosmological constraints from breaking growth degeneracy

Louis Perenon,[1,*] Stéphane Ilić,[2,3,4] Roy Maartens,[1,5] and Alvaro de la Cruz-Dombriz[6]

[1] *Department of Physics & Astronomy, University of the Western Cape, Cape Town 7535, South Africa*
[2] *Université PSL, Observatoire de Paris, Sorbonne Université, CNRS, LERMA, F-75014, Paris, France*
[3] *CEICO, Institute of Physics of the Czech Academy of Sciences, Na Slovance 2, Praha 8, Czech Republic*
[4] *IRAP, Université de Toulouse, CNRS, CNES, UPS, Toulouse, France*
[5] *Institute of Cosmology & Gravitation, University of Portsmouth, Portsmouth PO1 3FX, UK*
[6] *Cosmology & Gravity Group, Department of Mathematics & Applied Mathematics, University of Cape Town, Rondebosch 7701, Cape Town, South Africa*

The key probes of the growth of large-scale structure are its rate f and amplitude σ_8. Redshift space distortions in the galaxy power spectrum allow us to measure only the combination $f\sigma_8$, which can be used to constrain the standard cosmological model or alternatives. By using measurements of the galaxy-galaxy lensing cross-correlation spectrum or of the galaxy bispectrum, it is possible to break the $f\sigma_8$ degeneracy and obtain separate estimates of f and σ_8 from the same galaxy sample. Currently there are only a handful of such separate measurements, but even this allows for improved constraints on cosmological models. We explore how having a larger and more precise sample of such measurements in the future could constrain further cosmological models. We consider what can be achieved by a future nominal sample that delivers a $\sim 1\%$ constraint on f and σ_8 separately, compared to the case with a similar precision on the combination $f\sigma_8$. For the six cosmological parameters of ΛCDM, we find improvements of ~ 5–50% on their constraints. For modified gravity models in the Horndeski class, the improvements on these standard parameters are ~ 0–15%. However, the precision on the sum of neutrino masses improves by 65% and there is a significant increase in the precision on the background and perturbation Horndeski parameters.

I. INTRODUCTION

The growth of large-scale structure is sensitive to the theory of gravity and its measurement is a powerful test of the standard and alternative models of cosmology. It is characterised at the most basic level by the rate of growth $f = -d\ln D/d\ln(1+z)$, where $D(z)$ is the growth function of the linear matter density contrast, $\delta(z,\boldsymbol{k}) = D(z)\delta(z_{\rm in},\boldsymbol{k})/D(z_{\rm in})$, given an initial redshift $z_{\rm in}$. This rate governs the evolution of peculiar velocities, whose impact on the observed galaxy power spectrum is to introduce a redshift space distortion (RSD). Measurement of this anisotropy at redshift z delivers an estimate of $f(z)\sigma_8(z)$, where σ_8 fixes the amplitude of the matter density fluctuations. The degeneracy between f and σ_8 echoes the degeneracy between the linear galaxy bias and σ_8, and it cannot be broken via RSD power spectrum measurements alone.

The degeneracy can be broken by using an alternative observable in the galaxy sample that involves σ_8 or f. For example, combining RSD power spectrum measurements with galaxy-galaxy lensing measurements has produced separate estimates of f and σ_8 [1–3]. There are currently only a handful of such estimates, but even with only three separated data pairs, constraints on cosmological models improve noticeably [4]. Another way to break the degeneracy is by combining RSD measurements in the power spectrum and bispectrum [5].

Breaking the growth degeneracy is expected to break degeneracies between certain cosmological and modified gravity parameters. Here we confirm this expectation by computing the improvement in precision when using future separated measurements of f and σ_8 as compared to using the usual combined measurements $f\sigma_8$. We make forecasts for the standard ΛCDM model and for scalar-tensor theories in the Horndeski class [6], using the effective field theory (EFT) of dark energy [7, 8] (see [9] for a recent review and [10–17] for more general Horndeski forecasts).

II. MODELS

We consider two models to assess the constraining power of the different growth of structure quantities. The first is the standard cosmological model ΛCDM, whose free parameters are [18]

$$\{\Omega_{\rm b}h^2, \Omega_{\rm c}h^2, H_0, \tau, A_{\rm s}, n_{\rm s}, \Sigma m_\nu\}, \tag{1}$$

where the total neutrino mass $\sum m_\nu$ is equally shared by the three degenerate species.

For the second, we chose the popular benchmark for studies of alternative gravitational models [9] that are Horndeski theories [6]. They are the most general covariant scalar-tensor theories with direct second-order equations of motion. We use in particular their description of linear perturbations provided by the α-EFT basis [19]. See [19] for complete details of the construction of the action.

Observations suggest that the speed of gravitational waves is equal to that of light [20, 21]. This reduces the number of redshift-dependent functions in the effective

* perenon.louis@yahoo.fr, corresponding author

description that govern how modifications of gravity affects perturbations to three:

$\alpha_M(z)$ – evolution of the effective Planck mass;
$\alpha_B(z)$ – mixing between the metric and the DE field;
$\alpha_K(z)$ – kinetic energy of scalar perturbations.

Although α_K has virtually no effect on constraints from current data [16, 22], it needs to be included as a free parameter, since it regulates the propagation speed of DE perturbations. Setting it arbitrarily to zero could restrict the space of stable models and thus bias the constraints [16, 23].

The functional forms of $\alpha_I(z)$, $I = M, B, K$, are not given by the effective description. For simplicity, we use the effective DE parametrisation[19, 24] common in literature:

$$\alpha_I(z) = a_I \, \frac{\Omega_{\rm x}(z)}{\Omega_{\rm x,0}}. \tag{2}$$

We also allow for deviations from a ΛCDM background by using the Chevallier-Polarski-Linder (CPL) [25, 26] parametrisation for the effective dark energy (DE) equation of state of the Horndeski models:

$$w_{\rm x}(z) = w_0 + w_a \, \frac{z}{1+z} \, . \tag{3}$$

In summary, the Horndeki model we consider contains five additional free parameters with respect to ΛCDM

$$\left\{\Omega_{\rm b}h^2, \Omega_{\rm c}h^2, H_0, \tau, A_{\rm s}, n_{\rm s}, \Sigma m_\nu, w_0, w_a, a_M, a_B, a_K\right\}. \tag{4}$$

ΛCDM is recovered for $w_0 = -1$ and $w_a = a_M = a_B = a_K = 0$.

III. METHODOLOGY

The cosmological evolution of the models is computed using the Boltzmann code[1] `CLASS` [27], and its modified version[2] `hi_class` [28, 29]. The cosmological data – hereafter referred to as the "baseline" – contains the SDSS-II/SNLS3 Joint Light-curve Analysis (JLA) sample of SNIa [30], the BOSS baryon acoustic oscillation (BAO) measurements [31–33] and the Planck 2018 cosmic microwave background (CMB) data, the low- and high-multipole temperature and polarisation [18]. We choose not to include CMB lensing data, to avoid inconsistencies related to potential ΛCDM-dependent assumptions made during the lensing reconstruction.

Our aim is to focus on the gain from breaking growth degeneracy, rather than making realistic mocks and forecasts. In order to compare the constraining power of separated measurements of f and σ_8 with the combined measurements $f\sigma_8$, we simulate data for a nominal future galaxy sample that delivers a one percent precision for f, σ_8 and $f\sigma_8$. We assume a redshift range containing 10 measurements at $z = 0.1, 0.2, ..., 1$. The effects of extending the redshift range are studied in Section IV C. We anticipate that a Stage IV experiment conducting a spectroscopic galaxy count survey together with a weak lensing survey, such as Euclid [34], should be able to achieve close to 1% precision on $f\sigma_8$, f and σ_8, using Planck priors on standard cosmological parameters.

Whenever needed, the growth quantities are computed with `CLASS` or `hi_class`. In order to compare the constraints on the same footing and avoid non-linear model dependencies, we compute the growth quantities with the linear power spectrum only. The values of σ_8 are obtained via the usual weighted integral of the linear power spectrum and f is computed as the log derivative $f = -(1+z)d\ln\sigma_8/d\ln z$ for simplicity.

We use as fiducial parameters the best-fit values obtained from the baseline constraints for the ΛCDM and Horndeski models. Then we create three sets of mocks for both models (for f, σ_8 and $f\sigma_8$), each exactly centred on their fiducial, *i.e.* with no random variance added to the data. ΛCDM has been shown to lie in a corner of the parameter space of stable Horndeski models [24], i.e., ghost- and gradient-free models. When performing forecasts using Markov chain Monte Carlo (MCMC) methods, the stability priors can lead to a disfavouring of models lying close to the corner, purely due to volume effects and independently of their actual likelihood. Such considerations may have a significant effect on our results. This is hinted at for example by the highly irregular posteriors in the baseline case in Figure 3 (grey contours) and the mismatch between their maximum and the best-fit model (dotted lines), characteristic of non-negligible prior effects. We can however expect those effects to be mitigated when additional data is added to the analysis, due to the fact that our Horndeski fiducial model (derived from the baseline best-fit and used to produce our mocks) lies noticeably away from the "ΛCDM corner". Even if our MCMC explorations were impacted by such priors, this should not affect our conclusions since we always make statements regarding relative improvements.

IV. CONSTRAINTS

The sampling of all the considered likelihoods, as well as the computation of best-fit parameters, are performed using the publicly available[3] suite of codes ECLAIR [35]. It uses as its main sampling algorithm the affine-invariant ensemble method of [36] and contains a novel and robust maximiser with reliable convergence towards the global maximum of the posterior.

[1] www.class-code.net
[2] www.hiclass-code.net
[3] https://github.com/s-ilic/ECLAIR

	$f\sigma_8$	$f+\sigma_8$
$\Omega_\mathrm{b}h^2$	$0.02244^{0.00013}_{-0.00013}$	$0.02245^{0.00012}_{-0.00012}$
$\Omega_\mathrm{c}h^2$	$0.11918^{0.00062}_{-0.00063}$	$0.11904^{0.00048}_{-0.00048}$
H_0	$68.10^{0.32}_{-0.32}$	$68.17^{0.22}_{-0.22}$
τ	$0.0581^{0.0058}_{-0.0066}$	$0.0589^{0.0044}_{-0.0056}$
$\ln\left(10^{10}A_\mathrm{s}\right)$	$3.0509^{0.0106}_{-0.0121}$	$3.0524^{0.0075}_{-0.0104}$
n_s	$0.9671^{0.0034}_{-0.0034}$	$0.9673^{0.0031}_{-0.0031}$
Σm_ν	$0.0263^{0.0062}_{-0.0263}$	$0.0248^{0.0058}_{-0.0248}$

Table I. Mean and 68% confidence interval for ΛCDM parameters. The constraints are obtained by combining the baseline with the $f\sigma_8$ mock (middle column) and f and σ_8 mocks (right column).

	baseline + $f\sigma_8$ / baseline	baseline + $f+\sigma_8$ / baseline	baseline + $f+\sigma_8$ / baseline + $f\sigma_8$
$\Omega_\mathrm{b}h^2$	1.08	1.15	1.06
$\Omega_\mathrm{c}h^2$	1.66	2.16	1.30
H_0	1.55	2.26	1.46
τ	1.25	1.54	1.22
$\ln\left(10^{10}A_\mathrm{s}\right)$	1.40	1.77	1.26
n_s	1.16	1.27	1.09
Σm_ν	1.48	1.57	1.13

Table II. Precision ratios for ΛCDM parameters. See Section IV A for details.

A. ΛCDM

Marginalised posterior distributions are shown in Figure 1. The corresponding means and 68% confidence intervals are given in Table I, while Table II shows the gain in precision relative to baseline (first two columns) and for the separated growth measurements $f+\sigma_8$ relative to the standard $f\sigma_8$ measurements (last column). We define the precision as the inverse width of the 68% marginalised confidence interval rather than using relative errors, since the latter can become misleading when the mean values are close to zero (e.g., in the case of Σm_ν). In addition, comparing relative errors would also be biased when the mean values shift, as happens for the Horndeski models (see below).

Next-generation surveys are forecast to deliver improved constraints from high-precision RSD $f\sigma_8$ data (see e.g. [34, 37]). The triangle plots and the tables confirm this. Table II (first column) shows that the gain in precision ranges from $\sim 10\%$ for $\Omega_\mathrm{b}h^2$ up to more than $\sim 50\%$ for $\Omega_\mathrm{c}h^2, H_0$ and Σm_ν, when considering the addition of the mock data on $f\sigma_8$ with 1% relative error to current cosmological datasets.

As expected the constraints improve further with the split mock data on f and σ_8, each with a 1% relative error. This combination performs from 6% to almost 50% better. In particular, the precision on $\Omega_\mathrm{c}h^2$ and H_0 is more than doubled relative to the baseline data alone.

The improvement obtained from the split f and σ_8 data over $f\sigma_8$ (as quantified by the third column of Table II) does not lead to an equal increase in precision on all the parameters that were already well constrained with $f\sigma_8$ RSD data. As an example, we can compare Σm_ν and H_0. Adding $f\sigma_8$ data yields almost a 50% gain on Σm_ν, while the split $f+\sigma_8$ data further increases the precision by 13%. By contrast, H_0 precision first increases by 55% followed by another 46% with the splitting.

The growth probes f, σ_8, and $f\sigma_8$ have different sensitivities to each cosmological parameter, which explains the range of changes in precision. One way to examine those sensitivities is to start with the baseline-only constraints. Figure 2 shows the posterior distributions of f, σ_8 and $f\sigma_8$ at redshift $z=0.1$ as derived parameters versus the cosmological parameters[4]. Each posterior thus illustrates how a change in a given cosmological parameter impacts the values of the derived growth quantities, taking into account (i.e., marginalising over) the remaining cosmological parameters and how their values need to change to keep a decent fit to the data.

On the other hand, adding constraints on the growth quantities amounts to convolving their posteriors with a Gaussian distribution (with a width equal to 1% of the central value). This in turn may reduce the width of the posterior on cosmological parameters, depending on the amount of correlation between the two. It is thus expected that cosmological parameters that are highly correlated (i.e., thin tilted ellipses) with a given growth quantity in the baseline case, will show the best improvements after including measurements of that growth quantity.

From Figure 2 we find that Ω_b, Ω_c, H_0, n_s are better constrained by adding the f mock (green) to the baseline, while τ, A_s, Σm_ν are better constrained by adding the σ_8 mock (purple). This may appear counter to the common expectation that σ_8 is more sensitive to parameters affecting the power spectrum amplitude, while f is more sensitive to parameters affecting its shape. It is the correlations induced by the baseline constraints that are the decisive factor.

Let us consider an illustrative example from Figure 2: the 2D posterior of $\{f(0.1), H_0\}$ exhibits a high correlation (thin tilted ellipse), while that of $\{\sigma_8(0.1), H_0\}$ is

[4] We find the orientations of these posteriors (i.e., correlation factors between parameters) to change very little with redshift. Therefore we consider only $z=0.1$ for illustration, but our discussion applies to the other z.

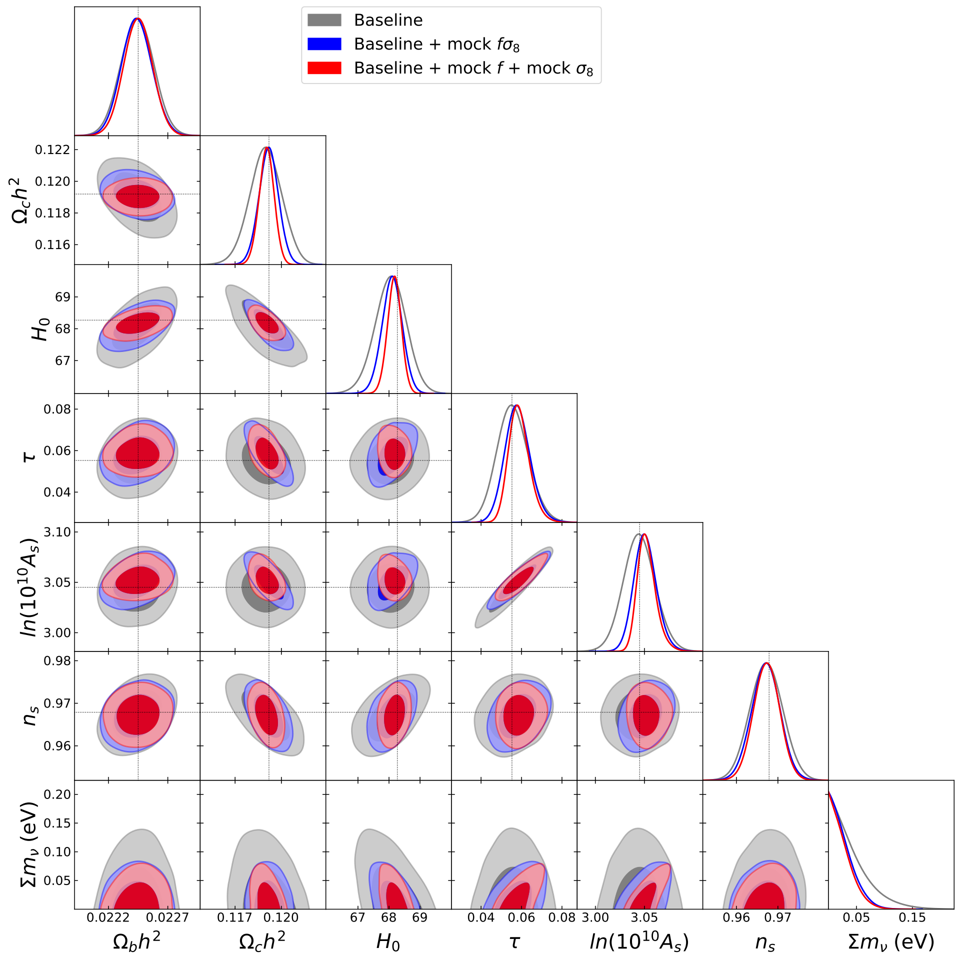

Figure 1. 1D and 2D marginalised posterior distributions for ΛCDM parameters derived from the baseline only (grey), baseline with mock on $f\sigma_8$ (blue) and baseline with mocks on f and σ_8 (red). The dotted lines indicate the parameter values for the fiducial model (corresponding to the baseline best-fit) used when generating mocks.

relatively irregular and close to an uncorrelated case. As a result, the addition of the f mock improves the H_0 constraint significantly more relative to the baseline (see the 1D posterior of H_0 in the top row of Figure 2).

These correlations can even lead to improved constraints on parameters that f and σ_8 should not depend on. An example is the tight constraint on the reionisation parameter τ produced by the mock on σ_8, which originates in the tight constraint on A_s from σ_8, combined with the underlying high correlation between A_s and τ, as shown in Figure 1. A tight constraint on τ is obtained even though it does not play a role in the value of σ_8.

B. Horndeski

The Horndeski parameter space is extended to include modifications in the background (w_0, w_a) and in the perturbations $(\alpha_M, \alpha_K, \alpha_B)$. Marginalised posterior distributions with the baseline and mock data sets are displayed in Figure 3, with the corresponding means and 68% confidence intervals in Table III. We observe that the maximum of the posterior distribution for the extension parameters shifts significantly towards the best-fit model (dotted lines), while the contours assume a much more regular, ellipsoidal shape compared to the baseline case. This is expected in a transition from a regime where priors still play a significant role (as discussed at the end of Section III), to a situation where data dominate the posterior.

Interestingly, these results also show that if the true underlying cosmology is indeed close to the Horndeski best-fit fiducial, then growth data with 1% relative precision (over the redshift range considered) could lead to the detection of this deviation from ΛCDM with strong significance (more than 5σ).

Table IV shows the gain in precision relative to baseline (first two columns) and for the separated growth measurements $f + \sigma_8$ relative to the standard $f\sigma_8$ measurements (last column). As pointed out earlier, the ki-

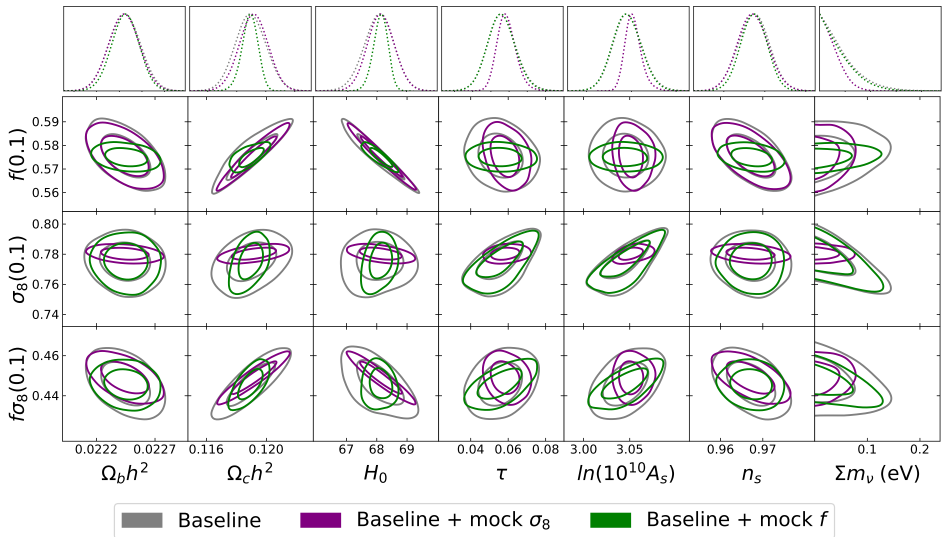

Figure 2. 1D marginalised posterior distributions (top row) for ΛCDM parameters, from baseline only (grey), baseline + mock on f (green) and baseline + mock on σ_8 (purple). Rows below show 2D posteriors of cosmological parameters against derived parameters f, σ_8 and $f\sigma_8$ at $z = 0.1$.

	$f\sigma_8$	$f + \sigma_8$
$\Omega_b h^2$	$0.02259^{0.00015}_{-0.00014}$	$0.02258^{0.00015}_{-0.00015}$
$\Omega_c h^2$	$0.11801^{0.00122}_{-0.00122}$	$0.11819^{0.00122}_{-0.00122}$
H_0	$68.44^{0.96}_{-0.96}$	$68.69^{0.85}_{-0.85}$
τ	$0.0508^{0.0075}_{-0.0075}$	$0.0526^{0.0070}_{-0.0068}$
$\ln(10^{10}A_s)$	$3.0324^{0.0157}_{-0.0155}$	$3.0366^{0.0140}_{-0.0136}$
n_s	$0.9704^{0.0042}_{-0.0042}$	$0.9702^{0.0042}_{-0.0042}$
Σm_ν	$0.0953^{0.0261}_{-0.0953}$	$0.0742^{0.0206}_{-0.0742}$
w_0	$-0.9636^{0.0862}_{-0.0797}$	$-0.9770^{0.0813}_{-0.0814}$
w_a	$-0.1901^{0.2632}_{-0.2636}$	$-0.1543^{0.2984}_{-0.2494}$
a_B	$1.9493^{0.1801}_{-0.2058}$	$1.9262^{0.1791}_{-0.2003}$
a_M	$3.3473^{0.4411}_{-0.5943}$	$3.0485^{0.2630}_{-0.3799}$

Table III. Mean and 68% confidence interval for Horndeski parameters. The constraints are obtained by combining the baseline with the $f\sigma_8$ mock (middle column) and f and σ_8 mocks (right column).

neticity coupling α_K is not constrained by the data and is therefore not included in the figure and tables. but a_K is included as a free parameter in the analysis. The accuracy that was gained on the cosmological parameters in ΛCDM is largely lost. Adding the mock on $f\sigma_8$ only delivers up to $\sim$20% precision gain (see Table IV). This can be attributed to the addition of new, poorly constrained degrees of freedom which naturally leads to larger errors on all the original parameters via correlations, as both sets may have similar and degenerate effects on the growth of structure. For example, Figure 3 shows how a_M and a_B are relatively degenerate with other parameters when using the baseline data only.

However, there is significant improvement for the extension parameters: adding future $f\sigma_8$ data yields a 230% improvement for the running of the effective Planck mass α_M and a remarkable $\sim$50% gain for Σm_ν. Even though $f\sigma_8$ is a probe of the perturbations, adding its mock to the baseline achieves a surprising $\sim$ 30% and $\sim$60% gain in precision for w_0 and w_a respectively.

The additional gain from disentangling f and σ_8 measurements is also subject to the effects of opening up the parameter space. The standard parameters see little improvement ($<$ 15%) over the $f\sigma_8$ case. By contrast, $w_a, \Sigma m_\nu$ and α_M precisions jump by a further $\sim$20%, $\sim$65% and $\sim$80% respectively.

The underlying reason that growth data provide such an enhancement on precision for the Horndeski parameters is rooted in the modification of gravitational dynamics (e.g., the Poisson equation) by α_I. As discussed in [4], these modifications produce two opposing contributions:

* a fifth force, enhancing growth;
* a higher effective Planck mass, suppressing growth.

The effective Planck mass is controlled solely by α_M for the models we consider. As a result, growth data strongly constrains a_M and also a_B. Table IV shows that the splitting of $f\sigma_8$ into f and σ_8 is very effective to further constrain a_M, thereby disentangling the fifth force and effective Planck mass contributions. This feature was seen even with current split data in [4].

The modified background parameters w_0, w_a con-

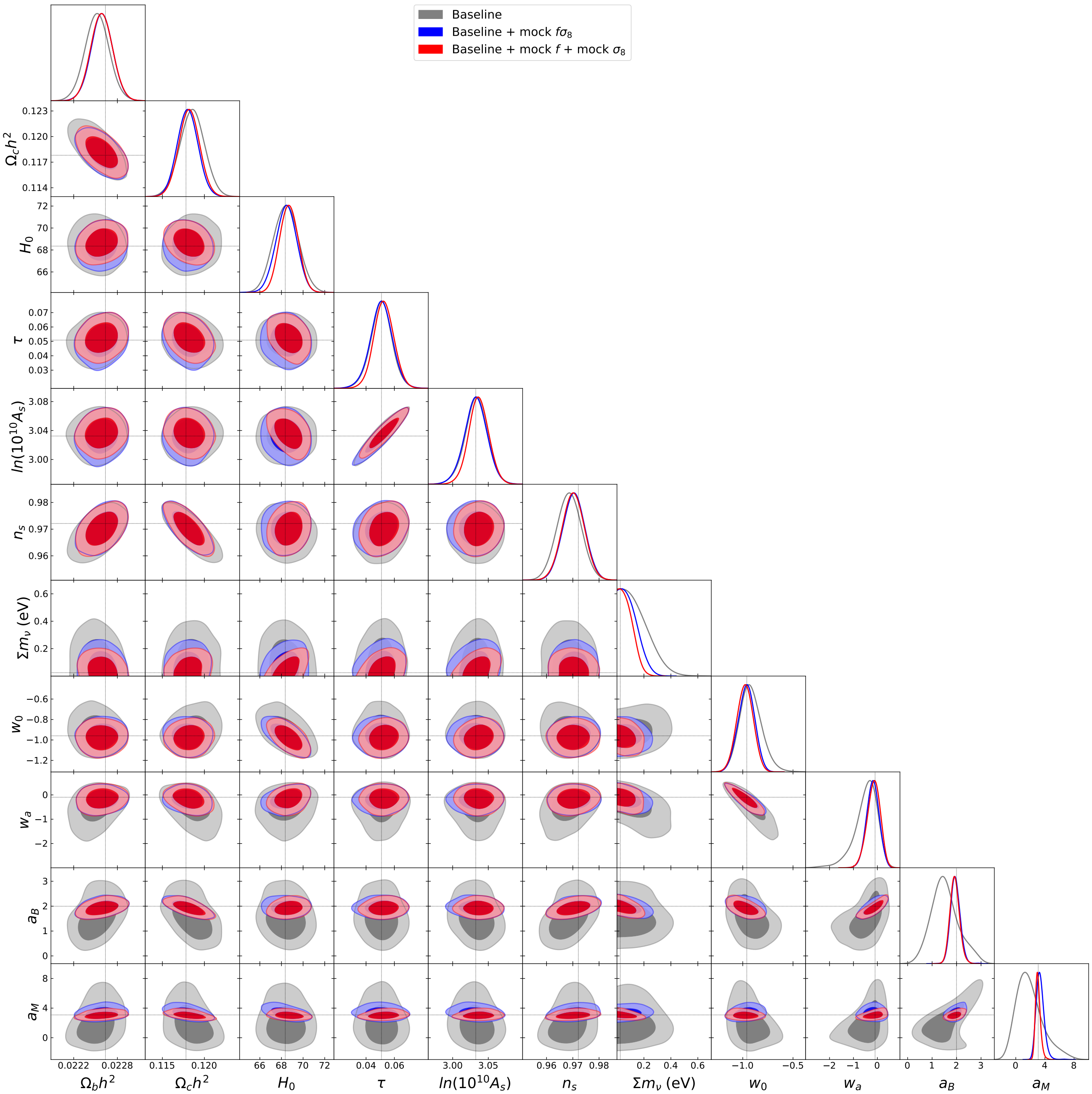

Figure 3. 1D and 2D marginalised posterior distributions for Horndeski parameters derived from the baseline only (grey), baseline with mock on $f\sigma_8$ (blue) and baseline with mocks on f and σ_8 (red). The dotted lines indicate the parameter values for the fiducial model (corresponding to the baseline best-fit) used when generating mocks.

tribute also to the growth of structure through the Hubble friction. Their effects on growth are therefore degenerate with those of α_I. We see in Figure 4 that w_0, w_a, a_B, a_M display some degeneracies in their 2D marginalised posteriors.

Following the arguments for ΛCDM, we can understand the separate improvements from f and σ_8 by analysing their posterior distributions versus cosmological parameters, shown in Figure 4. Note that the stability requirements for the Horndeski models induce highly non-Gaussian posterior distributions, which makes the analysis more subtle. Figure 4 shows that f correlates more strongly with a_B, a_M than σ_8, so that adding f measurements results in a larger increase in precision on these parameters. Since these two parameters control the strength of the fifth force, this could be expected, given that σ_8 is an integrated function of f, which tends to wash out the effects of the fifth force. Note that the fifth

	baseline + $f\sigma_8$ / baseline	baseline + f + σ_8 / baseline	baseline + f + σ_8 / baseline + $f\sigma_8$
$\Omega_b h^2$	1.11	1.10	0.99
$\Omega_c h^2$	1.20	1.20	1.00
H_0	1.19	1.35	1.12
τ	0.96	1.04	1.05
$\ln(10^{10} A_s)$	0.98	1.11	1.13
n_s	1.10	1.10	1.00
Σm_ν	1.49	1.91	1.65
w_0	1.29	1.32	1.01
w_a	1.65	1.59	1.18
a_B	2.83	2.87	1.03
a_M	3.30	5.32	1.77

Table IV. Precision ratios for Horndeski parameters. See Section IV B for details.

force is an effect occurring at low redshifts as opposed to the effect of the Hubble friction or neutrinos. A chain of correlations – seen in the baseline constraints – shows that σ_8 brings a larger gain in precision for w_0, w_a and Σm_ν. This signals therefore a higher sensitivity of σ_8 to modifications of gravity spanning longer periods.

It is in fact expected that the effect of neutrinos is partially degenerate with that of modified gravity (see e.g. [38, 39]). Massive neutrinos suppress the growth of structure on small scales, which can either oppose or reinforce modified gravity, depending on whether the fifth force or the Planck mass running is favoured. Horndeski models compatible with current RSD $f\sigma_8$ constraints produce a suppression of growth at late times [4].

The baseline constraints in Figure 3 show that the 2D posteriors of Σm_ν with a_B and a_M are fairly irregularly shaped , while those with w_0 and w_a are more correlated. More surprisingly, as noted above, Σm_ν has almost a 50% gain with the addition of the $f\sigma_8$ mock data, as in the case of ΛCDM. The splitting improves constraints by a further 70% as opposed to 7% in ΛCDM. It is therefore clear that these growth mocks break the neutrino-modified gravity degeneracy by constraining efficiently Σm_ν and the extension parameters. Figure 4 tells us that this is rooted in the correlation of Σm_ν with σ_8 in the baseline.

On the other hand, we also see that all the intricate degeneracies between the extension parameters and standard model parameters render the baseline constraints for the latter much less correlated than in the case of ΛCDM. This explains why the improvements from the splitting are not as great in the case of Horndeski for the other standard parameters.

Note that when the background evolution is fixed to that of ΛCDM, Σm_ν displays correlation with α_B [40]. Here, the freedom that arises from varying w_0, w_a lessens that correlation.

C. Extending the redshift range

Having understood better the influence of each mock data set on the constraints, we now assess the effect of extending the redshift coverage of the mocks. More specifically, we examine the respective merits of adding $f\sigma_8$ or $f + \sigma_8$ measurements, when extending the maximum redshift of each mock. Table V shows that the combined data $f\sigma_8$ with $z_{\max} = 2$ (first column) performs no better than $f + \sigma_8$ data with half the redshift range ($z_{\max} = 1$, see Tables I and III). We find that extending the redshift range further improves the precision up to 30% with respect to $z_{\max} = 1$ in the case of the combined mock $f\sigma_8$ for ΛCDM and Horndeski models, and respectively 20% and 15% in the case of f and σ_8 mocks.

V. CONCLUSION

Upcoming galaxy surveys such as Euclid [34] and SKA [37] with their unprecedented precision is a call to sharpen our tools for constraining gravity. One cosmological probe well-suited for that task is the growth of structure. This toolbox is further complemented by the releases of measurements on f and σ_8 [1–3, 5].

In this paper, we considered the performance that a future nominal galaxy sample can deliver with a ∼ 1% relative error on f and σ_8 separately and on the combination $f\sigma_8$. We compared the constraints from the separated data with those from the combination data. We assumed 10 measurements per growth quantity equally spread on the redshift range z = 0.1, 0.2, ..., 1.0. For the case of ΛCDM, the improvements in precision range over ∼5–50%. For modified gravity described by Horndeski models, the improvements on these standard model parameters reduce to ∼0–15%.

However, the splitting of f and σ_8 stands out as very effective in breaking the neutrino - modified gravity degeneracy, with the sum of neutrino masses enjoying an improvement of 65% over the case with only $f\sigma_8$ data. We find also a significant increase in the precision on the background and perturbation Horndeski parameters, with an additional gain of ∼20% for the varying effective DE equation of state parameter w_a and ∼ 80% for the evolution of the effective Planck mass a_M. Extending the redshift of the mocks up to $z_{\max} = 2$ shows that the constraints provided by the combined $f\sigma_8$ data are already matched by the split data f and σ_8 with $z_{\max} = 1$.

Our results highlight that growth data, whether split or combined, with 1% relative error could lead to the detection of deviations from ΛCDM with strong significance (more than 5σ), should the underlying cosmology be close to the current Horndeski best-fit fiducial.

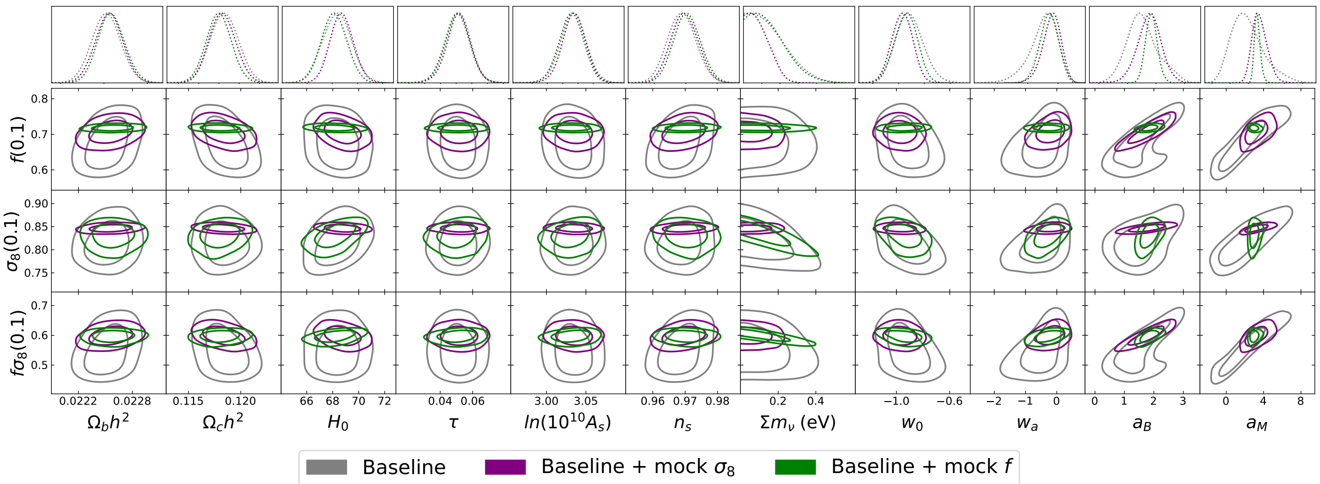

Figure 4. 1D marginalised posterior distributions (top row) for Horndeski parameters, from baseline only (grey), baseline + mock on f (green) and baseline + mock on σ_8 (purple). Rows below show 2D posteriors of cosmological parameters against derived parameters f, σ_8 and $f\sigma_8$ computed at $z = 0.1$.

The splitting of growth data on $f\sigma_8$ into data on f and σ_8 with galaxy-galaxy lensing [1–3] or by combinations with the bispectrum [5] emerges clearly from this work as both a powerful complementary probe for the standard model and a stringent probe to detect departures from it. The latter could prove crucial in the era of future surveys, given the current tensions within the standard model and the emergence of alternative models of gravity favoured via Bayesian evidence [41, 42].

ACKNOWLEDGEMENTS

We are grateful to Julien Bel for helpful exchanges and feedback on the draft. We thank Matteo Martinelli for useful discussions. The authors acknowledge the Sciama High Performance Compute Cluster, which is supported by the ICG at the University of Portsmouth, and the CHPC the Centre for High Performance Computing (CHPC), South Africa, for providing computational resources for this research project. LP and RM are supported by the South African Radio Astronomy Observatory (SARAO) and the National Research Foundation (Grant No. 75415). RM is also supported by the UK STFC Consolidated Grant ST/N000668/1. SI was supported by the European Structural and Investment Fund and the Czech Ministry of Education, Youth and Sports (Project CoGraDS - CZ.02.1.01/0.0/0.0/15_003/0000437). AdlCD acknowledges financial support from NRF Grants No.120390, Reference: BSFP190416431035 and No.120396, Reference: CSRP190405427545, Project No. FPA2014-53375-C2-1-P from the Spanish Ministry of Economy and Science, Project No. FIS2016-78859-P from the European Regional Development Fund and Spanish Research Agency (AEI), and support from Projects Nos. CA15117 and CA16104 from COST Actions EU Framework Programme Horizon 2020.

---

[1] S. de la Torre *et al.*, Astron. Astrophys. **608**, A44 (2017), arXiv:1612.05647 [astro-ph.CO].
[2] F. Shi *et al.*, Astrophys. J. **861**, 137 (2018), arXiv:1712.04163 [astro-ph.CO].
[3] E. Jullo *et al.*, Astron. Astrophys. **627**, A137 (2019), arXiv:1903.07160 [astro-ph.CO].
[4] L. Perenon, J. Bel, R. Maartens, and A. de la Cruz-Dombriz, JCAP **1906**, 020 (2019), arXiv:1901.11063 [astro-ph.CO].
[5] H. Gil-Marín, W. J. Percival, L. Verde, J. R. Brownstein, C.-H. Chuang, F.-S. Kitaura, S. A. Rodríguez-Torres, and M. D. Olmstead, Mon. Not. Roy. Astron. Soc. **465**, 1757 (2017), arXiv:1606.00439 [astro-ph.CO].
[6] G. W. Horndeski, Int. J. Theor. Phys. **10**, 363 (1974).
[7] G. Gubitosi, F. Piazza, and F. Vernizzi, JCAP **1302**, 032 (2013), [JCAP1302,032(2013)], arXiv:1210.0201 [hep-th].
[8] J. K. Bloomfield, E. A. Flanagan, M. Park, and S. Watson, JCAP **1308**, 010 (2013), arXiv:1211.7054 [astro-ph.CO].
[9] N. Frusciante and L. Perenon, Phys. Rept. **857**, 1 (2020), arXiv:1907.03150 [astro-ph.CO].
[10] J. Gleyzes, D. Langlois, M. Mancarella, and F. Vernizzi, JCAP **02**, 056 (2016), arXiv:1509.02191 [astro-ph.CO].
[11] D. Alonso, E. Bellini, P. G. Ferreira, and M. Zumalacarregui, Phys. Rev. **D95**, 063502 (2017), arXiv:1610.09290 [astro-ph.CO].
[12] J. S.-Y. Leung and Z. Huang, Int. J. Mod. Phys. D **26**, 1750070 (2017), arXiv:1604.07330 [astro-ph.CO].

	$f\sigma_8$ ($z_{\rm max}=2$)	$f+\sigma_8$ ($z_{\rm max}=2$)
$\Omega_b h^2$	$0.02245^{0.00012}_{-0.00012}$	$0.02244^{0.00012}_{-0.00012}$
$\Omega_c h^2$	$0.11910^{0.00055}_{-0.00054}$	$0.11907^{0.00046}_{-0.00046}$
H_0	$68.17^{0.25}_{-0.25}$	$68.17^{0.21}_{-0.21}$
τ	$0.0588^{0.0045}_{-0.0056}$	$0.0587^{0.0038}_{-0.0048}$
$\ln(10^{10}A_s)$	$3.0524^{0.0075}_{-0.0102}$	$3.0521^{0.0062}_{-0.0089}$
n_s	$0.9673^{0.0032}_{-0.0033}$	$0.9673^{0.0031}_{-0.0031}$
Σm_ν	$0.0234^{0.0055}_{-0.0234}$	$0.0234^{0.0055}_{-0.0234}$
$\Omega_b h^2$	$0.02259^{0.00015}_{-0.00015}$	$0.02258^{0.00015}_{-0.00015}$
$\Omega_c h^2$	$0.11813^{0.00123}_{-0.00123}$	$0.11824^{0.00117}_{-0.00117}$
H_0	$68.60^{0.88}_{-0.88}$	$68.63^{0.82}_{-0.81}$
τ	$0.0523^{0.0071}_{-0.0072}$	$0.0524^{0.0071}_{-0.0071}$
$\ln(10^{10}A_s)$	$3.0357^{0.0144}_{-0.0143}$	$3.0365^{0.0141}_{-0.0143}$
n_s	$0.9702^{0.0042}_{-0.0042}$	$0.9701^{0.0041}_{-0.0041}$
Σm_ν	$0.0656^{0.0181}_{-0.0656}$	$0.0693^{0.0185}_{-0.0693}$
w_0	$-0.9761^{0.0840}_{-0.0850}$	$-0.9764^{0.0705}_{-0.0710}$
w_a	$-0.1328^{0.2831}_{-0.2542}$	$-0.1452^{0.2666}_{-0.2167}$
a_B	$1.9494^{0.1710}_{-0.1939}$	$1.9266^{0.1594}_{-0.1857}$
a_M	$3.1274^{0.3142}_{-0.4618}$	$3.0552^{0.2409}_{-0.3672}$

Table V. Mean and 68% confidence interval for ΛCDM (top) and Horndeski (bottom) parameters with the redshift of the mocks extended to $z = 0.1, 0.2, ..., 2.0$. The constraints are obtained by combining the baseline with the $f\sigma_8$ mock (middle column) and f and σ_8 mocks (right column).

[13] K. N. Abazajian *et al.* (CMB-S4), (2016), arXiv:1610.02743 [astro-ph.CO].
[14] R. Reischke, A. Spurio Mancini, B. M. Sch afer, and P. M. Merkel, Mon. Not. Roy. Astron. Soc. **482**, 3274 (2019), arXiv:1804.02441 [astro-ph.CO].
[15] A. Spurio Mancini, R. Reischke, V. Pettorino, B. Sch afer, and M. Zumalacárregui, Mon. Not. Roy. Astron. Soc. **480**, 3725 (2018), arXiv:1801.04251 [astro-ph.CO].
[16] N. Frusciante, S. Peirone, S. Casas, and N. A. Lima, Phys. Rev. **D99**, 063538 (2019), arXiv:1810.10521 [astro-ph.CO].
[17] M. Ballardini, D. Sapone, C. Umiltà, F. Finelli, and D. Paoletti, JCAP **05**, 049 (2019), arXiv:1902.01407 [astro-ph.CO].
[18] N. Aghanim *et al.* (Planck), (2019), arXiv:1907.12875 [astro-ph.CO].
[19] E. Bellini and I. Sawicki, JCAP **1407**, 050 (2014), arXiv:1404.3713 [astro-ph.CO].
[20] B. Abbott *et al.* (LIGO Scientific, Virgo), Phys. Rev. Lett. **119**, 161101 (2017), arXiv:1710.05832 [gr-qc].
[21] B. Abbott *et al.* (LIGO Scientific, Virgo, Fermi-GBM, INTEGRAL), Astrophys. J. **848**, L13 (2017), arXiv:1710.05834 [astro-ph.HE].
[22] E. Bellini, A. J. Cuesta, R. Jimenez, and L. Verde, JCAP **1602**, 053 (2016), [Erratum: JCAP1606,no.06,E01(2016)], arXiv:1509.07816 [astro-ph.CO].
[23] C. D. Kreisch and E. Komatsu, JCAP **1812**, 030 (2018), arXiv:1712.02710 [astro-ph.CO].
[24] F. Piazza, H. Steigerwald, and C. Marinoni, JCAP **1405**, 043 (2014), arXiv:1312.6111 [astro-ph.CO].
[25] M. Chevallier and D. Polarski, Int. J. Mod. Phys. **D10**, 213 (2001), arXiv:gr-qc/0009008 [gr-qc].
[26] E. V. Linder, Phys. Rev. Lett. **90**, 091301 (2003), arXiv:astro-ph/0208512 [astro-ph].
[27] D. Blas, J. Lesgourgues, and T. Tram, JCAP **1107**, 034 (2011), arXiv:1104.2933 [astro-ph.CO].
[28] M. Zumalacarregui, E. Bellini, I. Sawicki, J. Lesgourgues, and P. G. Ferreira, JCAP **1708**, 019 (2017), arXiv:1605.06102 [astro-ph.CO].
[29] E. Bellini, I. Sawicki, and M. Zumalacarregui, (2019), arXiv:1909.01828 [astro-ph.CO].
[30] M. Betoule *et al.* (SDSS), Astron. Astrophys. **568**, A22 (2014), arXiv:1401.4064 [astro-ph.CO].
[31] F. Beutler, C. Blake, M. Colless, D. H. Jones, L. Staveley-Smith, L. Campbell, Q. Parker, W. Saunders, and F. Watson, Mon. Not. Roy. Astron. Soc. **416**, 3017 (2011), arXiv:1106.3366 [astro-ph.CO].
[32] L. Anderson *et al.* (BOSS), Mon. Not. Roy. Astron. Soc. **441**, 24 (2014), arXiv:1312.4877 [astro-ph.CO].
[33] A. J. Ross, L. Samushia, C. Howlett, W. J. Percival, A. Burden, and M. Manera, Mon. Not. Roy. Astron. Soc. **449**, 835 (2015), arXiv:1409.3242 [astro-ph.CO].
[34] L. Amendola *et al.*, Living Rev. Rel. **21**, 2 (2018), arXiv:1606.00180 [astro-ph.CO].
[35] S. Ilić, M. Kopp, C. Skordis, and D. B. Thomas, (2020), arXiv:2004.09572 [astro-ph.CO].
[36] D. Foreman-Mackey, D. W. Hogg, D. Lang, and J. Goodman, Publ. Astron. Soc. Pac. **125**, 306 (2013), arXiv:1202.3665 [astro-ph.IM].
[37] D. J. Bacon *et al.* (SKA), Publ. Astron. Soc. Austral. **37**, e007 (2020), arXiv:1811.02743 [astro-ph.CO].
[38] B. S. Wright, K. Koyama, H. A. Winther, and G.-B. Zhao, JCAP **06**, 040 (2019), arXiv:1902.10692 [astro-ph.CO].
[39] M. Ballardini, M. Braglia, F. Finelli, D. Paoletti, A. A. Starobinsky, and C. Umiltà, (2020), arXiv:2004.14349 [astro-ph.CO].
[40] N. Bellomo, E. Bellini, B. Hu, R. Jimenez, C. Pena-Garay, and L. Verde, JCAP **1702**, 043 (2017), arXiv:1612.02598 [astro-ph.CO].
[41] S. Peirone, G. Benevento, N. Frusciante, and S. Tsujikawa, Phys. Rev. D **100**, 063540 (2019), arXiv:1905.05166 [astro-ph.CO].
[42] J. Solà Peracaula, A. Gomez-Valent, J. de Cruz Pérez, and C. Moreno-Pulido, Astrophys. J. **886**, L6 (2019), arXiv:1909.02554 [astro-ph.CO].